Small crack formation in a low carbon steel with banded ferrite–pearlite structure

N. Narasaiah, K.K. Ray*

Department of Metallurgical and Materials Engineering, Indian Institute of Technology, Kharagpur 721302, India

Abstract

The phenomenon of the formation of small cracks in a banded plain carbon steel has been studied on dumble-shaped plate type specimens under varied cyclic stress amplitudes at the load ratio of $R = 0$. The locations at which the cracks were found to nucleate could be classified as: (i) ferrite–pearlite interface (FPI), (ii) ferrite–ferrite grain boundary (FFGB), (iii) ferrite grain body, and (iv) inclusion–matrix interface. The most preferred site for such crack nucleation in the investigated steel was found to be the ferrite–pearlite interface. The orientation of the initiated small cracks was found to vary widely between $0°$ and $90°$ with respect to the loading direction unlike some earlier reported results. It is reported here for the first time that the angle between the direction of banding and the loading axis has pronounced effect on the orientation of such small cracks. The lengths of these cracks at FPI and FFGB are found to be larger than the ones nucleated inside ferrite grain body. The preferred site of crack nucleation and the influence of the banding on the size and the orientation of the small cracks have been explained using inhomogeneous distribution of stress/strain in the microstructure and incompatible strains along the interfaces.
© 2004 Elsevier B.V. All rights reserved.

Keywords: Fatigue; Crack initiation; Small crack; Banded structure; SA333 steel

1. Introduction

Micro-crack nucleation in structural materials is considered to be the first stage in fatigue damage, which is consequently followed by small/short and macro crack propagation leading to critical fatigue fracture. Any crack with all three dimensions small is defined here as "small crack" [1]; the short cracks, on the other hand, are known to possess two small dimensions and the third one of macroscopic size. A substantial body of evidence, accumulated over the last two decades, un-ambiguously indicates that small or short cracks exhibit faster growth at low stress intensity factor range (ΔK) than what would be predicted from the propagation of macro cracks [1–5]. Such evidences are also well supplemented by a large number of investigations [6–8] related to the possible mechanisms of crack nucleation. By now it is well conceived that a large percentage of fatigue life of smooth specimens are spent in the domain of crack nucleation and small/short crack

growth, in the emerging clean (i.e., with very low inclusion content) structural materials especially in high cycle fatigue. It is thus imperative to gather more knowledge about crack nucleation and about small/short crack growth behaviour in such structural materials. In a recent communication, two of the present authors have extended some understanding about the influence of microstructure on the short crack growth behaviour in a structural steel [9], whereas in the present communication the role of microstructure on crack nucleation in a low carbon steel is being addressed.

The pre-macro crack regime of fatigue damage is often termed as "fatigue crack initiation stage". It is well known by now that the microstructure of a material significantly influences this stage of fatigue damage. But unfortunately it is difficult to demarcate the crack nucleation stage from the stage of small/short crack propagation in this regime. The existing models that describe small/short crack growth behaviour in materials do account for the microstructural features (e.g., grain boundaries, precipitates, second phase particles, etc. [10–12]). The developments related to the mechanisms of crack nucleation, on the other hand, are found to be mostly

* Corresponding author. Tel.: +91 3222 283278; fax: +91 3222 282280.
  E-mail address: kkrmt@metal.iitkgp.ernet.in (K.K. Ray).

associated with concepts related to sub-structural features (e.g., dislocations, dislocation-vacancy complexes, dislocation dipoles, etc. [13,14]). Information related to the role of microstructure on micro crack nucleation are limited and scattered, and such information have not led to any organised conceptual developments plausibly because of the numerous variety of microstructures encountered in the different investigated materials. The earlier attempts to probe this aspect have usually laid more emphasis either on the investigated material system or on the mechanics of small/short crack growth rather than trying to achieve a generalised perspective on the effect of microstructure on the location of crack nucleation. The present study aims to achieve understanding about the location and characteristics of small cracks in a two-phase material.

In this pursuit, this article deals with the formation of small cracks in a commercial steel exhibiting ferrite–pearlite structure. The material selected for this study is a SA333 grade 6 steel, which is used in the primary heat transport system of pressurized heavy water reactors. The major aim of this report is to identify the preferred crack nucleation sites in this material. In addition, the selected steel of engineering importance exhibits banded microstructure. The existing literature does not indicate the role of such structures on the nucleation of small cracks; this has been examined in this study. This report further aims to reveal the possible mechanisms associated with each type of crack observed in the material.

2. Experimental procedure

The steel used in this investigation is SA333 grade 6, which is used for the construction of piping for the primary heat transport system of pressurized heavy water reactors. The chemical composition of the steel is shown in Table 1. Samples for microstructural studies were prepared on sections oriented both to the longitudinal and the transverse directions of the pipe axis. These samples were initially ground
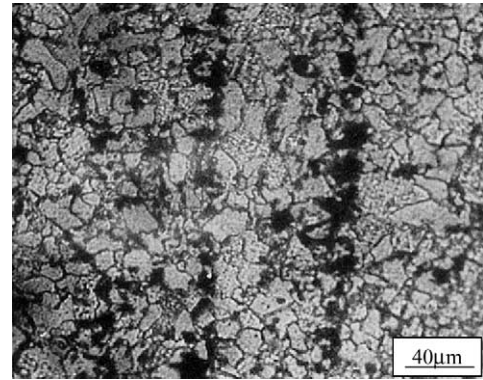
Table 1
Chemical composition of the investigated steel (in weight percentage)

Element	Composition
C	0.14
Mn	0.9
Si	0.25
P	0.016
S	0.018
Al	<0.1
Cr	0.08
Ni	0.05
V	<0.01
N	0.01
Cu	0.05
Pb	80 ppm
H	<5 ppm
O	0.03
Fe	Balance

Fig. 1. Typical banded microstructure of the investigated material.

with emery paper and were then polished first using alundum and finally using 0.25-μm diamond paste. The size and the number of inclusions on the polished specimens were found to be so insignificant that quantitative estimations of their size and volume fraction by conventional standard procedure like JIS G0555 [15] were found to be difficult. The polished samples were then etched with 2% nital solution to reveal the microstructure. Optical microscopic examination indicated that the steel contained ferrite and pearlite with prominent banding as shown in Fig. 1. The banding indices were determined following the procedure described in ASTM standard E-1268 [16], and were found to be 0.053 and 0.018 in the longitudinal and the transverse directions, respectively.

The tensile properties of the material were determined on specimens having their axis parallel to the length of the pipe. Round tensile specimens of 5-mm gauge diameter and 20-mm gauge length were fabricated from the as-received plates following ASTM standard E8-93 [17]. The tests were carried out using a Universal testing machine (Schimadzu, model: AG-5000G) at a nominal strain rate of $4.2 \times 10^{-4}\,\text{s}^{-1}$ at room temperature. The average yield and tensile strength of the material were found to be 292 and 433 MPa, respectively, whereas the uniform and the total elongation were estimated as 23 and 46%, respectively.

The fatigue studies were carried out on small hourglass type flat specimens, made from the as-received material as shown in Fig. 2. One of the flat surfaces of each of these
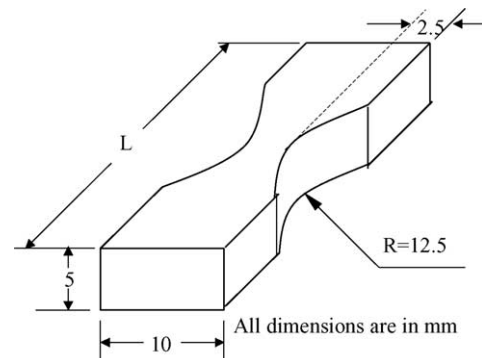

Fig. 2. Specimen configuration used for small crack initiation studies.

Table 2
Test details for crack initiation studies in the investigated steel

Sp. code	Cross-section area ($W \times T$) (mm × mm)	Applied stress range × σ_y	Number of cycles applied	Banding direction with respect to loading
Sp-LR01	5.54 × 5.00	0–0.6	2.0×10^4	Parallel
Sp-LR02	4.92 × 5.04	0–0.7	2.0×10^4	Parallel
Sp-LR03	5.04 × 4.74	0–0.8	2.0×10^4	Parallel
Sp-LR04	5.02 × 4.74	0–0.9	2.0×10^4	Parallel
Sp-LR05	6.10 × 5.02	0–1.0	2.0×10^4	Parallel
Sp-LR06	5.03 × 6.18	0–0.9	3.0×10^4	Parallel
Sp-LR07	6.12 × 6.7	0–0.9	1.0×10^4	Parallel
Sp-CL01	4.80 × 4.92	0–0.6	2.0×10^4	Perpendicular
Sp-CL02	4.88 × 4.90	0–0.8	2.0×10^4	Perpendicular
Sp-CL03	4.92 × 4.90	0–1.0	2.0×10^4	Perpendicular

samples was ground, polished, and etched to reveal the microstructure in a manner similar to the procedure described earlier. The fatigue tests were performed with the help of an Instron machine (model: 8501) operated at various stress levels ranging from 0.6 to 1.0 of yield stress (σ_y) maintaining the minimum stress as zero. These tests were conducted using sinusoidal wave at a frequency of 10 Hz at room temperature (approximately 298 K) in the laboratory air. A series of such tests were made not only at different load levels but also for different number of cycles (10^4, 2×10^4, and 3×10^4) and for different variations in sample orientation, so that the cyclic loading is done both parallel and perpendicular to the banding direction of the microstructure. The details of each test together with the dimensions of the specimens are shown in Table 2. After the fatigue test, all the specimens were examined under a scanning electron microscope (JEOL model: 5800) to locate the crack initiation sites. A series of photographs with careful demarcation of the loading direction were taken from numerous locations of interest, which exhibited small cracks. The average length of the small cracks and their location in the microstructure with respect to the loading direction were next examined.

3. Results and discussion

The locations at which cracks initiate in a microstructure and the nature of such cracks after a stage of development where these can be conveniently examined by scanning electron microscopy, are the primary content of this study. The cracks, thus, examined may be simply termed as "small cracks". In order to understand the influence of the microstructure on the nature of the initiated cracks, the fatigue tests have been carried out in such a manner that the small cracks are generated with almost negligible growth. The size range of the observed cracks was found to be 1–37 μm. This range is considered natural, because when one type of crack gets generated with the lower bound values of the stated size range, some alternate cracks are found with sizes near the upper bound, nucleated under identical stress range and identical number of imposed fatigue cycles. A series of these cracks were photographed using a scanning electron microscope at

suitable magnifications so that their maximum dimension can be measured conveniently.

An attempt to classify the documented cracks indicated that their locations in the microstructure are significantly governed by the presence of interfaces, inclusions and inhomogeneities. The observed small cracks can be broadly categorized into four types based on the position at which these are located in the microstructure. The classified different initiation sites are:

(a) ferrite–pearlite interface (FPI),
(b) ferrite–ferrite grain boundary (FFGB),
(c) ferrite grain body, and
(d) inclusion–matrix interface.

3.1. Crack initiation at ferrite–pearlite interface

A random scanning of various locations (on the specimen surface) to reveal the different types of cracks during SEM examination indicated that the occurrence of ferrite–pearlite interface cracks is much higher (approximately 10 times) than that of the other types of cracks. Some typical ferrite–pearlite interface cracks are shown in Fig. 3. The FPI cracks in this figure are indicated by arrows. The size and orientation of these cracks with respect to the loading axis were analyzed. Within the investigated stress ranges and the applied number of cycles, the observed cracks were found to exhibit random sizes. This implies that when the number of cycles is changed from 1.0×10^4 to 3.0×10^4 or the stress range is changed from 0.6 to 0.9 of σ_y the crack lengths do not vary significantly. However, an increase in the number of cycles or the maximum stress amplitude leads to a higher number of crack nucleation sites. All the observed cracks can be strictly termed as microstructurally small because these were not found to cross any ferrite grain boundary or ferrite–pearlite interface.

The size distribution of the recorded ferrite–pearlite interface (FPI) cracks is shown in Fig. 4. The average length and the associated standard deviation of the FPI cracks were estimated as 8.6 ± 3.4 μm. One can note from Fig. 4 that the highest population of cracks occurs in the size range 5–15 μm. An alternate analysis indicates that cracks generated in specimens having the loading axis parallel to the banding in the
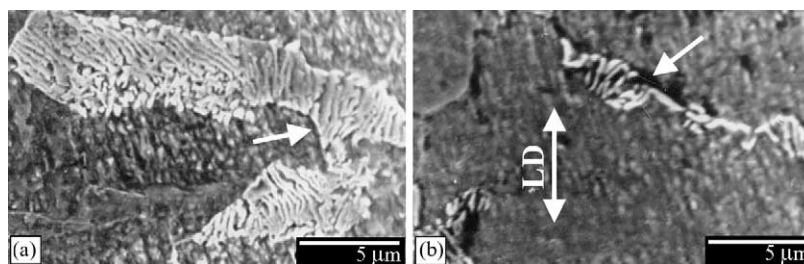
Fig. 3. Two typical ferrite–pearlite interface cracks. The loading direction (LD) common to both the figures is marked in (b).

microstructure are smaller compared to the crack lengths in specimens having the loading axis perpendicular to the banding direction. This aspect has been illustrated using inserts showing the size distribution for these cracks in Fig. 4. The mean sizes of cracks in specimens having banding parallel and perpendicular to loading direction are $7.0 \pm 1.9\,\mu m$ and $11.0 \pm 3.8\,\mu m$, respectively. Hence, it can be concluded that length of cracks in specimens having banding direction perpendicular to the loading axis is higher compared to that in specimens having banding direction parallel to loading axis.

An analysis of the orientation of the cracks with respect to loading direction in both types of specimens (i.e., parallel and perpendicular banding with respect to loading axis) indicates that these can widely vary between $0°$ and $90°$. This observation is not in agreement with the results reported by Liu et al. [18] and Zhang et al. [6], who have indicated that such angles primarily lie between $45°$ and $90°$. Zhang et al. [6] have not mentioned about any banding in the microstructure of the low-carbon steel they have investigated, whereas Liu et al. [18] have studied on polycrystalline copper. It is considered here that the observed difference in the nature of

the crack-orientation arises from the banded microstructure. In order to probe this phenomenon in depth, the distribution of the orientation of the cracks with respect to loading axis for both types specimens were examined in Fig. 5. The results in this figure reveal that (i) when banding is parallel to loading direction, cracks are mostly oriented between $0°$ and $45°$ and (ii) when banding is perpendicular to loading axis cracks are mostly oriented between $45°$ and $90°$. The latter observation is in agreement with some earlier reported results [6,18]. It can thus be inferred that (a) FPI cracks are relatively smaller in size and their orientation with respect to loading direction remains between $0°$ and $45°$ when banding is parallel to loading direction, and (b) these cracks are larger in size and their orientation with respect to loading direction remains in the range from $45°$ to $90°$ when banding is perpendicular to loading axis. Hence, it can be concluded that microstructural banding significantly influences the size and orientation of small cracks in the investigated steel at the stage of their nucleation. This is the first information of its kind.
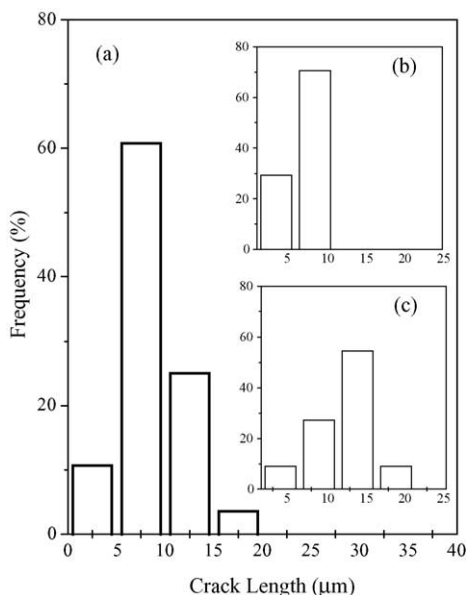

Fig. 4. Size distribution of (a) all ferrite–pearlite interface cracks, (b) cracks in samples having banding parallel to loading direction, and (c) cracks in samples having banding perpendicular to loading direction.
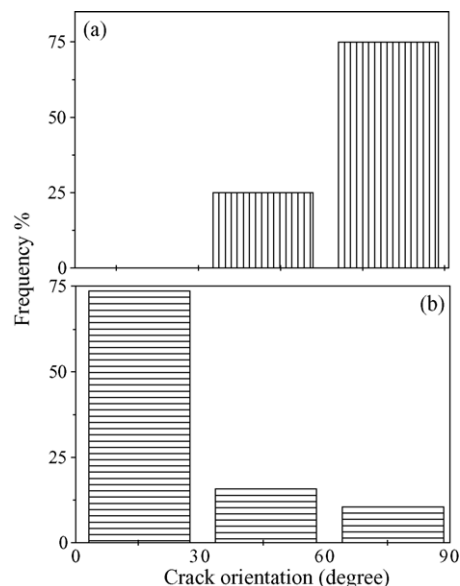

Fig. 5. Distribution of the orientation of ferrite–pearlite interface cracks in (a) specimens exhibiting banding perpendicular to loading axis and (b) specimens exhibiting banding parallel to loading axis. The orientation of a crack has been estimated with respect to the loading axis.
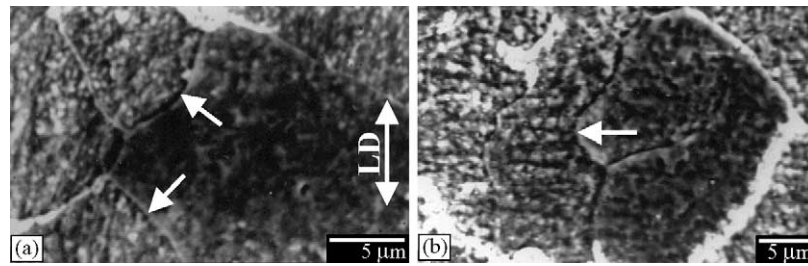
Fig. 6. A set of typical ferrite–ferrite grain boundary cracks. The loading direction (LD) common to both the figures is marked in (a).

3.2. Crack initiation at ferrite–ferrite grain boundary

The preference for nucleation of fatigue cracks at ferrite–ferrite grain boundaries were found to be next to that at FPI. Some typical ferrite–ferrite grain boundary (FFGB) cracks are shown in Fig. 6. The analyses of FFGB cracks were made in a similar manner to that of FPI cracks. The size distribution of these cracks is shown in Fig. 7 whereas the distribution of the orientation of the cracks with respect to loading axis for both types of specimens are shown in Fig. 8. The results in Fig. 8(a) and (b) correspond to observations made on specimens having banding direction perpendicular and parallel to the loading axis respectively. An analysis of the size and orientation of these cracks infer:

(i) the mean size of the estimated FFGB cracks is $8.3 \pm 4.0 \, \mu m$;
(ii) the average sizes of the cracks in specimens having banding parallel and perpendicular to the loading direction are $6.0 \pm 2.2 \, \mu m$ and $10.5 \pm 4.1 \, \mu m$, respectively;
(iii) when banding is parallel to the loading axis, these cracks are mostly oriented with angles of 0–$45°$ to the loading axis;
(iv) when banding is perpendicular to the loading axis the FFGB cracks subtend angles between $45°$ and $90°$ with the loading axis.

The above inferences lead to the conclusion that the effect of microstructural banding on the nature and orientation of small cracks initiated at FFGB and at FPI is similar. The
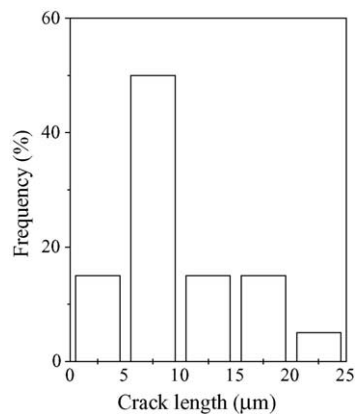

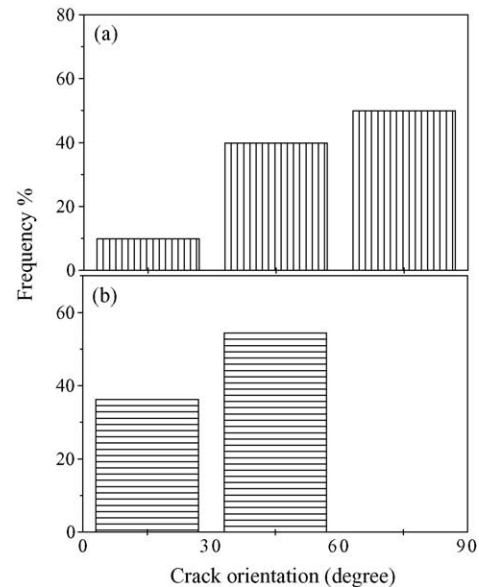Fig. 7. Size distribution of the ferrite–ferrite grain boundary cracks.

Fig. 8. Distribution of the orientation of ferrite–ferrite grain boundary cracks in (a) specimens exhibiting banding perpendicular to loading axis and (b) specimens exhibiting banding parallel to loading axis. The orientation of a crack has been estimated with respect to the loading axis.

observations related to FPI and FFGB cracks can thus be generalized with the contentions that (a) interface crack sizes are smaller for specimens having banding parallel to the loading axis compared to that for specimens having banding perpendicular to the loading axis, and (b) these cracks are associated with angles between $0°$ and $45°$ for the former type of specimen, unlike that between $45°$ and $90°$ for specimens having banding direction perpendicular to the loading axis. In general, the average length of the FFGB cracks are smaller than those initiated at FPI.

3.3. Crack initiation in ferrite grain body

Several cracks nucleated in the ferrite grain body were also found in the investigated steel, but their number was considerably less than those initiated at FPI and FFGB. Fig. 9 shows some typical small cracks initiated in the ferrite grain body. The distribution of the size and the orientation of these cracks are shown in Figs. 10 and 11, respectively. The average (ferrite grain body) crack lengths for both types of loading were found to be $5.8 \pm 2.5 \, \mu m$, whereas the variation of the
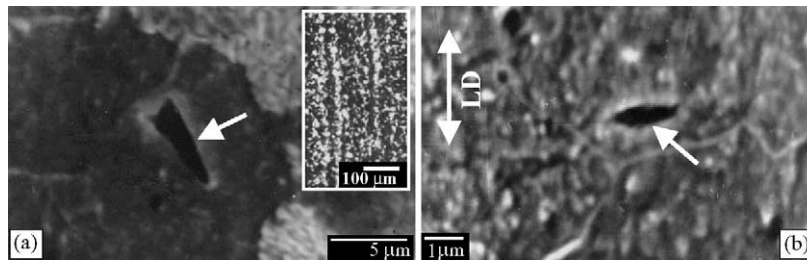
Fig. 9. Some typical ferrite grain body cracks. The microstructural banding is shown as an insert to indicate its orientation with respect to loading direction (shown as a double sided arrow).
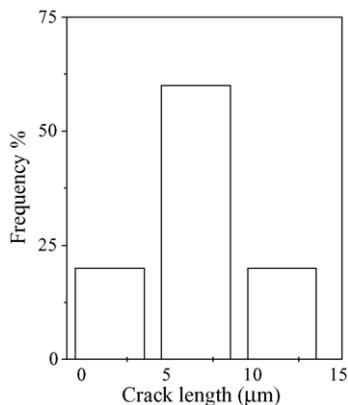

Fig. 10. Size distribution of the ferrite grain body cracks.

average orientation of the cracks owing to the different types of loading was found to be marginal; for the banding direction parallel and perpendicular to the loading axis, these were found to be $48.6 \pm 27.7°$ and $58.8 \pm 24.5°$, respectively. Interestingly the influence of the variation of the loading axis
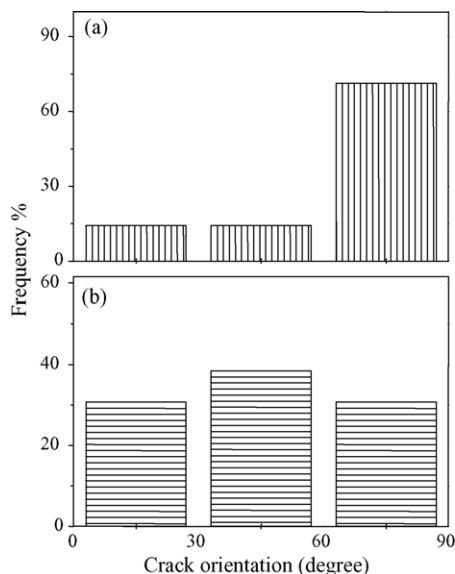

Fig. 11. Distribution of the orientation of ferrite grain body cracks in (a) specimens exhibiting banding perpendicular to loading axis and (b) specimens exhibiting banding parallel to loading axis. The orientation of a crack has been estimated with respect to the loading axis.

with respect to the direction of banding was found to be negligible on the nature of the ferrite grain body cracks.

Some salient characteristics of the grain body cracks are: (a) these are wider but smaller in length compared to the cracks nucleated at ferrite–ferrite or ferrite–pearlite interfaces, (b) these exhibit some specific shapes like elliptical or nail-type, and (c) one end of these cracks was almost always found near the ferrite–ferrite grain boundary or near the ferrite–pearlite interface.

3.4. Crack initiation at inclusions

It is considered in general that inclusions are the most preferred sites for crack nucleation. But the number of inclusion-associated cracks (IAC) was found to be negligible compared to the FPI, FFGB, and grain body cracks. As an example, in each sample approximately $40\,mm^2$ area were randomly scanned to locate IAC at magnifications of $2000–5000\times$. Such a search in 12 samples could lead to the detection of only five inclusion-associated cracks. This phenomenon is in agreement with the very low inclusion content of the investigated nuclear grade steel. Two typical inclusion-associated cracks are shown in Fig. 12 and details of the size and orientation of IAC are compiled in Table 3. It is difficult to comment about the distribution of size and orientation of this type of cracks from these few observations. But it was found that these cracks always initiate along the inclusion length irrespective of the specific angle between the loading axis and the banding direction. Crack initiation at inclusions generally occurs by the separation of the relatively weak interface between the matrix and the inclusion. This also causes formation of this type of cracks along the longer dimension of inclusions.

Table 3
Details of the size and the orientation of the inclusion-associated cracks

Sl. No.	No. of cycles	Stress $\times \sigma_y$	Crack length (μm)	Orientation[a] (°)
1.	1.1×10^4	0.9	36	30
2.	1.1×10^4	0.9	18.8	90
3.	2.0×10^4	0.8	5.8	55
4.	2.0×10^4	0.8	3.6	44
5.	2.0×10^4	0.8	11.7	56

σ_y: yield strength.
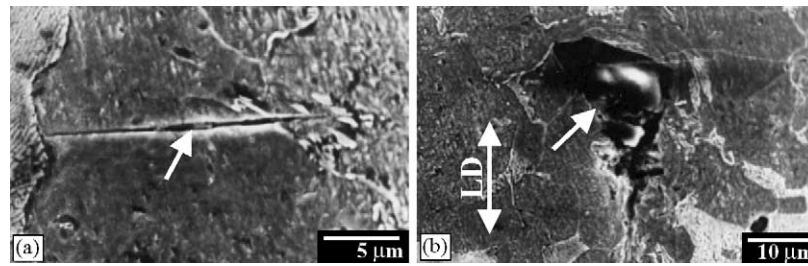[a] With respect to loading direction.

Fig. 12. Two typical cracks nucleated at inclusions: (a) crack propagation perpendicular to loading direction and (b) crack propagation along the loading direction.

3.5. On the crack initiation sites in low carbon steels

The examination of crack initiation sites in the 0.14% C steel with ferrite–pearlite microstructure indicates the order of preference for the site of crack initiation as: ferrite–pearlite interface, ferrite–ferrite grain boundary and ferrite grain body excluding the insignificant occurrence of crack initiation at inclusion–matrix interfaces. These observations are compared with a few similar examinations by earlier investigators. Tokaji et al. [19,20] have reported that crack initiation and propagation in low carbon steel occur through grain boundaries. However, these investigators have not distinguished between crack initiation sites at ferrite–pearlite interface and ferrite–ferrite grain boundary. Zhang et al. [6] have observed during low cycle impact loading of a 0.1% C steel that the most favourable site for crack nucleation is grain boundary. So the present observations of preferred crack initiation at ferrite–pearlite interfaces and at grain boundaries are in agreement with the above observations. However, Tokaji et al. [20] have found that cracks usually occur in ferrite grains when the grain size is finer, but these get initiated at grain boundaries in coarse-grained materials. These inferences have been derived by Tokaji et al. [20] from experimental results on a steel heat-treated to exhibit ferrite grain size of 24 μm (fine) and 84 μm (coarse). In the present investigation ferrite grain size is found to be only 12 μm and hence following the report of Tokaji et al., one would expect preferred crack nucleation in grain body in contrast to what has been observed. Rios et al. [8], on other hand, have observed that crack initiation occurs only along the slip bands inside the ferrite phase of a 0.4% C steel.

Based on the earlier and the present observations of crack initiation sites in carbon steels, one can infer that preferable crack initiation site in this material can be either grain body or grain boundary/interface. However, it is not clear which factors significantly govern the preference for a specific crack initiation site. It is known from some earlier studies [21,22] that the mechanical state of the ferrite phase and the pearlite colony in ferrite–pearlite structures vary with the carbon content of steel and such variations can also be expected to be influenced by the grain size of the material. It is inferred here that the preference for grain body or grain boundary/interface cracks is governed by the mechanical state of the ferrite phase and that of the pearlite colony in steels. It may also be addi-

tionally expected that the formation of the slip bands in the ferrite phase should get dictated by this aspect. In this investigation, slip bands have not been observed even when the fatigue samples were examined at considerably high magnifications: for example one can examine the photograph of the ferrite grain body cracks in Fig. 9. This contrasts with the view rendered by Rios et al. (Fig. 3 of [8]) and Zhang et al. (Fig. 4 of [6]). But observations of grain boundary/interface crack formation without being preceded by slip bands are found reported in the literature [23,24].

3.6. On the mechanism of crack initiation in the investigated steel

Slip bands impinging against grain boundary or interfaces has been suggested by Zhang et al. [6] as the primary cause for the formation of interface cracks. Such impingements usually result in several micro-splits leading to the formation of small cracks. In the current study, slip line impingement causing micro-splits could not be detected. An alternate possibility for the nucleation of the interface cracks could be due to considerable incompatibility between the elastic and the plastic deformation in the vicinity of an interface [7]. It is considered here that such incompatibility in deformation is also capable of yielding split type cracks with their subsequent coalescence to form small cracks. In Fig. 3(b) one can observe a few split-cracks around the ferrite–pearlite interface, but no distinct slip lines. Hence, it is inferred that the mechanism of formation of the small cracks at ferrite–pearlite interface in the investigated steel is predominantly governed by incompatible elastic–plastic deformation around the interfaces.

Using optical interferometric measurements of slip step heights at grain facets in fatigued copper, Kim and Laird [25] noted that fatigue cracks may nucleate at grain boundaries if: (i) the grain boundaries are separated by highly misoriented grains, (ii) the active slip system of at least one of the grains is directed at the intersection of the boundary with the specimen surface, and (iii) the traces of the high angle grain boundaries in the free surface make a large angle (30–90°) with the tensile stress axis. In general, grain boundary cracking may arise from one of two mechanisms during cyclic loading: (a) at low to intermediate plastic strain amplitude, the impingement of persistent slip bands (PSBs) at grain boundaries causes cracking [26,27], and (b) at high plastic strain amplitudes, grain

boundary cracking occurs as a consequence of surface steps formed at the boundary [29]. In this study, impingement of persistent slip bands at FFGBs has not been recorded and hence the nucleation of FFGB cracks can be attributed to the possible formation of surface steps at grain boundaries. The latter can be considered to originate from elastic–plastic incompatibility strains existing at FFGBs associated with wide orientation difference between the adjacent grains.

The grain body cracks are popularly considered to occur at persistent slip bands [6,8]. Since slip bands could not be detected in the ferrite phase of the investigated steel under the employed experimental conditions, any operative mechanism involving slip bands is thus naturally ruled out. The formation of the grain body cracks can be explained by the existence of an inhomogeneous stress or strain distribution inside ferrite. Such inhomogeneity in the stress/strain distribution is known [21,22] to be intense near the grain boundary and this is believed to be the cause for the formation of these cracks as well as for one end of these cracks remaining close to the interface of ferrite–pearlite or ferrite–ferrite grain boundary. The inhomogeneity in the stress/strain distribution has been reported by Ankem and Margolin [28] and Ray and Mondal [22] using experimental results on two-phase microstructures.

The possibility of crack initiation due to elastic or elastic–plastic incompatibility near grain boundaries and at ferrite–pearlite interfaces can be suitably assessed if the local stress/strain distribution is known. Due to the difficulty of generating such data, an attempt is made here to understand the role of elastic or elastic–plastic incompatibility in a qualitative manner. In elastically anisotropic phases like ferrite or iron-carbide, incompatibility in stress would develop across grain boundaries or phase interfaces, if the strains across these are considered continuous. The variation in local stresses can be considerable in iron since its relative degree of elastic anisotropy is 2.512 [29]; this implies that shear modulus can vary by this factor in this metal depending on the direction of shear elements within the lattice. In order to understand the degree of variation in local stresses along the ferrite–pearlite interfaces in a similar manner, information is required about the modulus values in different directions of the orthorhombic iron-carbide. Since these values are not available in the literature, it is considered here that the degree of elastic anisotropy at ferrite–pearlite interface would be higher than the relative degree of anisotropy of iron (2.512, [29]) and hence it can be assumed to be multiple of 2.512. Considering the minimum multiplication factor to be the ratio of shear modulii of iron (81.6 GPa, [29]) and that of iron-carbide (70 GPa, [30]), which is 82:70, the elastic incompatibility at ferrite–pearlite interface would be at least ≈2.94. The high degree of elastic anisotropy in ferrite and at ferrite–pearlite interfaces may thus be attributed to be the cause for crack initiation at these locations in the investigated microstructures.

Further considering a bicrystal of ferrite–ferrite or ferrite pearlite colony (Fig. 13) under a uniform tensile stress and following the report of Hu et al. [7], one of the compatible
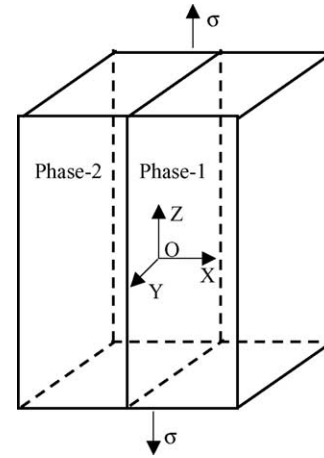

Fig. 13. Geometry of a planar interface between two-phase domains, the interface being parallel to the loading axis.

elastic or the plastic strain conditions can be written as

$$\Delta \in_{xx}^{e} = \, \in_{xx}^{e,1} - \, \in_{xx}^{e,2} = 0 \tag{1}$$

$$\Delta \in_{xx}^{pl} = \, \in_{xx}^{pl,1} - \, \in_{xx}^{pl,2} = 0 \tag{2}$$

where $\Delta \in_{xx}^{e}$ is the change in elastic strain along x–x, $\in_{xx}^{e,1}$ the elastic strain in phase-I along x–x, $\in_{xx}^{e,2}$ the elastic strain in phase-II along x–x, $\Delta \in_{xx}^{pl}$ the change in plastic strain along x–x, $\in_{xx}^{pl,1}$ the plastic strain in phase-I along x–x, and $\in_{xx}^{pl,2}$ is plastic strain in phase-I along x–x.

Usually $\in_{xx}^{e,1}$ (or $\in_{xx}^{pl,1}$) is different from $\in_{xx}^{e,2}$ (or $\in_{xx}^{pl,2}$) in the vicinity of grain boundary or at the interface between ferrite phase and pearlite colony. This physical condition leads to additional internal stresses, termed here as "incompatible internal stress" to full-fill the continuity requirement. A mismatch between the "incompatible internal stresses" or that in strain components along a grain boundary or an interface leads to the cracking of ferrite–ferrite grain boundary or the ferrite–pearlite interface. The FPI cracks in Fig. 3 and FFGB cracks in Fig. 6 are considered to arise due to this reason. The observation of higher number of FPI cracks and their larger lengths compared to those of FFGB cracks is thus attributed to the fact that $\Delta \in_{xx}^{e}$ or $\Delta \in_{xx}^{pl}$ is higher in magnitude for FPI cracks than that of FFGB cracks. The higher possible variation of shear modulus in the ferrite–pearlite interface than that along ferrite–ferrite grain boundaries supports this contention. The elastic and the plastic strains depicted in the compatible strain conditions given by Eqs. (1) and (2) are simplified versions based on a bi-crystal model. The elastic and the plastic strains of the near neighbourhood grains are expected to influence these equations. However, the qualitative explanation for the higher number of FPI cracks and their larger lengths compared to those of FFGB cracks by the "incompatible internal stress" concept using the bi-crystal model can be considered rational.

4. Conclusions

The results of the present investigation and their related discussion lead to the conclusions: (i) cracks nucleate at four locations, i.e, ferrite–pearlite interface, ferrite–ferrite grain boundary, inside ferrite grain body, and at inclusion in the investigated microstructure of SA333 steel, (ii) ferrite–pearlite interfaces and ferrite–ferrite grain boundaries are found as significantly preferred crack initiation sites in comparison to ferrite grain body in the investigated steel, (iii) the lengths of small crack initiated at ferrite–pearlite interfaces are usually larger in size compared to those at other locations, (iv) the orientation of the cracks with respect to the loading axis ranges widely between $0°$ and $90°$ in the banded microstructure unlike that between $45°$ and $90°$ reported in ferrite–pearlite microstructures by a few earlier investigators, (v) the direction of banding in a ferrite–pearlite microstructure with respect to loading axis exerts prominent influence on the size of the small cracks, and (vi) elastic or elastic–plastic incompatibility is suggested to be the primary mechanism for crack initiation at the interfaces and at the ferrite grain boundaries in the investigated steel.

Acknowledgments

References

[1] R.O. Ritchie, J. Lankford (Eds.), Small Fatigue Cracks, The Metallurgical Society Inc., New York, 1986.

[2] S. Suresh, R.O. Ritchie, Int. Metals Rev. 29 (1984) 445–476.

[3] K.J. Miller, E.R. de los Rios (Eds.), The Behaviour of Short Fatigue Cracks, EGF1, Mechanical Engineering Publications, London, 1986.

[4] K.J. Miller, E.R. de los Rios (Eds.), The Short Fatigue Cracks, ESIS-13, Mechanical Engineering Publications, London, 1992.

[5] K.S. Ravichandran, R.O. Ritchie, Y. Murakami (Eds.), Small Fatigue Cracks: Mechanics, Mechanisms and Applications, Elsevier Science Publications, 1999.

[6] M. Zhang, P. Yang, T. Yuxu, Int. J. Fatigue 21 (1999) 823–830.

[7] Y.M. Hu, W. Floer, U. Krupp, H.J. Crist, Mater. Sci. Eng. A278 (2000) 170–180.

[8] E.R. De Los Rios, H.J. Mohamed, K.J. Miller, Fatigue Fract. Eng. Mater. Struct. 8 (1985) 49–63.

[9] K.K. Ray, N. Narasaiah, R. Sivakumar, Mater. Sci. Eng. A 372 (2004) 81–90.

[10] K.S. Chan, J. Lankford, Scripta Metallurgica. 17 (1983) 529–532.

[11] A. Navarro, E.R. de los Rios, Fatigue Fract. Eng. Mater. Struct. 11 (1988) 383–396.

[12] K. Hussain, E.R. de los Rios, A. Navarro, Eng. Fract. Mech. 44 (1993) 425–436.

[13] U. Essman, U. Gosele, H. Mughrabi, Philos. Mag. A 44 (1981) 405–426.

[14] J.G. Antonopoulos, L.M. Brown, A.T. Winter, Philos. Mag. 34 (1976) 549–563.

[15] Japanese standard JISG-0555, Microscopic Testing Method for the Non-metallic Inclusions of steels, 1992.

[16] E1268-94, Annual Book of ASTM Standards, vol. 03.01, 1993, pp. 812–838.

[17] E8-93, Annual Book of ASTM Standards, vol. 03.01, 1993, pp. 130–149.

[18] H.W. Liu, M. Bayerlein, H. Mughrabi, A. Day, P.N. Quested, Acta Metall. Mater. 40 (1992) 1763–1771.

[19] K. Tokaji, Int. J. Fatigue 16 (1994) 571–578.

[20] K. Tokaji, T. Ogawa, Y. Harada, Fatigue Fract. Eng. Mater. Struct. 9 (1986) 205–217.

[21] K.K. Ray, D. Mondal, Acta Metall. et Materialia 39 (1991) 2201–2208.

[22] K.K. Ray, D. Mondal, Met. Trans. 23A (1992) 3309–3315.

[23] S. Kocanda, Fatigue Failure of Metals, Sijthoff and Noordhoff International Publishers, 1978, p. 113.

[24] J. Awatani, K. Katagiri, Bull. JSME 12 (1969) 10–18.

[25] W.H. Kim, C. Laird, Acta Metall. 26 (1978) 789–799.

[26] J.C. Figueroa, C. Laird, Mater. Sci. Eng. 60 (1983) 45–58.

[27] H. Mughrabi, R. Wang, K. Differt, U. Essman, in: J. Lankford, D.L. Davidson, W.L. Morris, R.P. Wei (Eds.), STP 811, American Society for Testing and Materials, Philadelphia, PA, 1993, pp. 5–45.

[28] S. Ankem, H. Margolin, Met. Trans. 17A (1986) 2209–2226.

[29] R.W. Herzberg, Deformation and Fracture Mechanics of Engineering Materials, 15, fourth ed., John Wiley & Sons, Singapore, 1996, pp. 7, 15.

[30] H. Mizubayashi, S.J. Li, H. Yumoto, M. Shimotomai, Scripta Materialia. 40 (1999) 773–777.